AJPS

Research Article

e-ISSN: 2980-0463

https://dergipark.org.tr/tr/pub/anatphar

In Silico Evaluation of a Novel Biphenyl-Triazole Derivative as a Potential CYP51 Inhibitor: A Molecular Docking Study

Ebru Sert, İnönü University, Faculty of Pharmacy, Malatya, Türkiye

Harun Uslu, Department of Pharmaceutical Chemistry, Faculty of Pharmacy, Firat University, Elâzığ, Türkiye

Bünyamin Göktaş, Department of Pharmaceutical Chemistry, Faculty of Pharmacy, Fırat University, Elâzığ, Türkiye

Zeynep Özdemir, İnönü University, Faculty of Pharmacy, Malatya, Türkiye, (Corresponding Author), zeynep.bulut@inonu.edu.tr

Citation Sert, E. , Uslu, H., Göktaş, B. & Özdemir, Z. (2026). In silico evaluation of a novel biphenyl-triazole derivative as a potential CYP51 inhibitor: A molecular docking study. *Anatolian Journal of Pharmaceutical Sciences, 5*(3), 185-203.

doi 10.71133/anatphar.1991144

Submission Date: July 18, 2026 - Acceptance Date: October 7, 2026 - Published Date: October 27, 2026

Abstract

Azole antifungals act by inhibiting fungal lanosterol 14α-demethylase (CYP51), and the spread of azole resistance, particularly among non-albicans Candida species, makes new CYP51-targeted compounds necessary. Here, the novel biphenyl–triazole derivative 1-(2-([1,1′-biphenyl]-4-yl)-2-(benzyloxy)ethyl)-1H-1,2,4-triazole (BTE1), designed to combine a heme-coordinating triazole ring with a hydrophobic biphenyl substituent, was evaluated computationally. BTE1 was built and energy-minimised with the MM2 force field (ChemOffice Professional 15.0), and its R- and S-enantiomers were docked with AutoDock 4.2.6 (50 runs per ligand) into Candida albicans CYP51 (PDB: 5FSA, 5V5Z) and, as a comparative model, Mycobacterium tuberculosis CYP51 (1EA1); the co-crystallised azoles fluconazole, itraconazole and posaconazole served as references, and redocking validated the protocol, reproducing the experimental poses with RMSD values of 0.99, 1.56 and 1.44 Å for fluconazole/1EA1, itraconazole/5V5Z and posaconazole/5FSA, respectively. Physicochemical, drug-likeness and ADME properties were predicted with SwissADME. Both enantiomers occupied the active site and interacted with the heme group, with S-BTE1 consistently giving slightly more favourable scores and estimated Ki values than R-BTE1 in all three models. The best predicted affinity was obtained against 5V5Z (−10.33 kcal/mol; estimated Ki 27.01 nM for S-BTE1), whereas in 1EA1 R- and S-BTE1 scored −10.14 and −10.24 kcal/mol versus −7.07 kcal/mol for fluconazole. π–π, π–cation and hydrogen-bonding interactions with key active-site residues and the heme were observed, and the predicted ADME profile complied with commonly applied drug-likeness criteria. These findings identify BTE1, particularly its S-enantiomer, as a promising scaffold, but they are purely predictive; enzymatic and antifungal assays are required to confirm CYP51 inhibition and biological activity..

Keywords: Azole antifungals, CYP51, molecular docking, biphenyl-triazole, antifungal resistance, in silico.

İNÖNÜ UNIVERSITY PRESS

Anatolian Journal of Pharmaceutical Sciences is a peer-reviewed open access journal. © 2026 The Author(s). OPEN ACCESS

1 INTRODUCTION

The immunocompromised patient population such as organ transplantation, hematological malignancies and groups with secondary immunodeficiency after COVID-19 are the fastest growing risk pool for invasive fungal infections worldwide. Invasive candidiasis caused by *Candida albicans* and non-albicans Candida species still remains one of the unsolved issues in clinical microbiology for this patient population with high death rates [1,2] .

The main therapeutic approach is based on azole drugs (voriconazole and fluconazole), which act by inhibiting the sterol 14α-demethylase (CYP51) enzyme, necessary for the synthesis of ergosterol, a compound responsible for the structural integrity of the fungal cell membrane (Figure 1) [3,4].

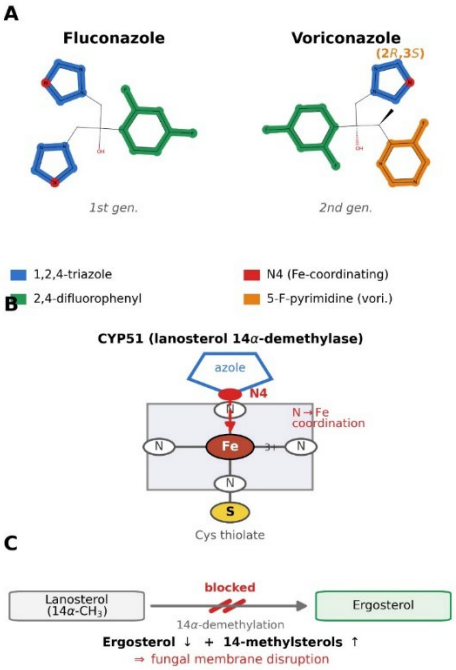

Figure 1. The structure and acting mechanism of voriconazole and fluconazole.

The mechanism of inhibition is based on the coordination of the nitrogen atom of the azole ring to the heme iron group at the active site of the enzyme, together with hydrophobic/Van der Waals interactions with residues such as TYR76, PHE78, PHE83, PHE255, and ALA256. A recent study showed that the addition of large aromatic side chains to the imidazole backbone improved the binding to the hydrophobic pocket of the enzyme and showed a better antifungal effect compared to fluconazole. This highlights the key role of this residue network in the design of pharmacophores (5,6) .

However, the therapeutic window for these classic azoles is gradually narrowing. Acquired resistance, stemming from overexpression of efflux pumps (CDR1, MDR1) and ERG11 mutations in the target enzyme (hotspots such as Y132F, K143R), combined with environmental selection pressure fueled by agricultural azol use, has reached a clinical bottleneck (7). The most visible face of this crisis is *Candida auris*, which has gained "superfungus" status since its identification in 2009 due to its disinfectant resistance and persistence on hospital surfaces; current systematic reviews show that 84,941 cases of colonization or infection have been reported in 82 countries across 6 continents worldwide, and fluconazole resistance has reached rates approaching 90% in isolated strains [4,8,9].

In light of this situation, drug discovery strategies are evolving along two axes. The first is structural classes that exhibit high selectivity on fungal CYP51 but do not bind to human CYP orthologs. Tetrazole-based oteseconazole (VT-1161) is a concrete example of this approach that has received clinical approval: on April 28, 2022, it made history as the first and only tetrazole-based antifungal approved by the US FDA to reduce the incidence of recurrent vulvovaginal candidiasis in women without reproductive potential; its low human-CYP affinity allowed it to eliminate the risk of drug-drug interactions [8]. The equivalent of this selectivity principle in the protozoa field is the β-phenyl-imidazole derivative VNI: the compound achieved a 100% cure rate in acute and chronic *Trypanosoma cruzi* infections induced by the Tulahuen strain with 30 days of oral administration at a dose of 25 mg/kg, while its efficacy against the resistant Y strain was limited to a peak parasitemia reduction ranging from 91-99% depending on the strain and administration protocol — this limitation motivated the development of the second-generation analog VFV [9]. The second axis is hybrid/dual-target designs where a single drug blocks both the ergosterol pathway and resistance mechanisms; CYP51-HDAC dual inhibitors have been shown to exhibit strong antifungal activity both in vitro and in vivo against azole-resistant clinical isolates and to suppress efflux pump function, yeast-hyphae morphological transition, and biofilm formation [10].

The design of BTE1 follows directly from the structural comparison between short-tailed and long-tailed azoles. The 1,2,4-triazole ring was retained as the pharmacophoric stabilizing, since coordination of an azole nitrogen to the heme iron is the conserved and non-negotiable requirement for CYP51 inhibition. In fluconazole, the remaining substituents are a second triazole ring and a 2,4-difluorophenyl group, neither of which extends appreciably into the hydrophobic substrate access channel; the binding of fluconazole is therefore concentrated around the heme and a small number of aromatic residues. Long-tailed azoles such as itraconazole and posaconazole, and the recently described long-arm amide-linked series, occupy this channel and retain activity in the presence of substitutions that reduce fluconazole binding [11-13].

In BTE1, one of the polar arms of the bis-triazole scaffold was therefore replaced by a biphenyl unit, chosen as a smaller, conformationally rigid and metabolically robust surrogate of such an extended hydrophobic tail. The benzyloxy linker positions the biphenyl group towards the access channel while preserving the geometry required for heme coordination, and introduces a stereogenic centre that provides a defined handle for subsequent stereochemical optimisation of the series. To our knowledge, this particular combination of a benzyloxy-linked biphenyl unit with a 1,2,4-triazole ring has not previously been evaluated against fungal CYP51.

The aim of the present study is therefore to characterise the predicted binding mode and relative affinity of BTE1 towards fungal CYP51 by molecular docking, and to establish, together with an in silico ADMET assessment, whether the compound merits the synthetic effort required for experimental evaluation.

By aligning its chiral center on a biphenyl-triazole scaffold with the heme-near hydrophobic pocket (TYR76/PHE255 region) of fungal CYP51, BTE1 seeks to achieve a functionally similar selectivity target via a different chemical pathway, whereas VFV provides high affinity to protozoa-specific CYP51 with a single chiral center on an oxadiazole-benzamide scaffold. Structure-based molecular docking (CADD), which forecasts binding affinity and interaction profile before synthesis, is the primary instrument speeding up this structural optimization process. Nevertheless, none of the three

approaches mentioned above such as high selectivity (VT-1161), functional irreversibility (VNI/VFV), and dual-targeting, offer a family of chiral azoles that combines fungal-specific selectivity with resistance-overcoming ability on the same scaffold. In order to close this gap, the design of BTE1, a chiral biphenyl-triazole derivative, and its in silico binding behavior on CYP51 are presented in this study. The primary goal of the study is to characterize the binding affinity and selectivity profile of BTE1 towards fungal CYP51 via molecular docking, thereby establishing a design template for a new series of chiral antifungal agents intended to overcome the structural limitations of existing azoles.

2 MATERIAL AND METHODS

2.1 Ligand Preparation

The candidate molecule BTE1 [1-(2-([1,1'-Biphenyl]-4-yl)-2-(benzyloxy)ethyl)-1*H*-1,2,4-triazole] was shown and subjected to three-dimensional optimization utilizing ChemOffice Professional 15.0 software. Energy minimization was conducted via the MM2 force field prior to docking simulations. BTE1 contains one stereogenic centre at the benzylic position. Both enantiomers, *R*-BTE1 and *S*-BTE1, were constructed and optimised separately, and both were subjected to docking; the results for both are reported. The co-crystallised ligands fluconazole (TPF470), itraconazole (1YN), and posaconazole (X2N), present in the corresponding CYP51 crystal structures, were used as reference compounds for docking and redocking validation.

2.2 Preparation of Target Protein

The crystal structures of Candida albicans CYP51 (PDB IDs: 5FSA and 5V5Z) and Mycobacterium tuberculosis CYP51 (PDB ID: 1EA1) were selected for molecular docking analysis [14-16]. The 1EA1 structure, which represents the first experimentally determined CYP51 structure, was included as a comparative model, whereas 5FSA and 5V5Z were used as the primary C. albicans CYP51 targets. The corresponding co-crystallised ligands, namely posaconazole (X2N) in 5FSA, itraconazole (1YN) in 5V5Z, and fluconazole (TPF470) in 1EA1, were retained from the respective crystal structures and used as reference ligands for docking and redocking validation. Redocking of these ligands was performed using the same docking protocol applied to BTE1 to assess the reliability of the docking procedure. All proteins were prepared with AutoDock Tools and Maestro (Schrödinger, LLC): water molecules were removed, polar hydrogen atoms were added, and

Gasteiger charges were assigned. The heme group was retained as part of the receptor.

The crystal structure of *Mycobacterium tuberculosis* CYP51 in complex with fluconazole (TPF470) (PDB ID: 1EA1) was analyzed to characterize the interaction profile of the co-crystallised ligand within the CYP51 active site. Previous structural and computational studies have identified several residues in the CYP51 active site as important for ligand binding, including TYR76, PHE78, MET79, PHE83, ARG96, ALA256, LEU321, and the heme group (HEM460). When hydrogen-bond, aromatic, hydrophobic, sulfur–π, carbon–π, and heme-coordination interactions are considered, TYR76, PHE78, PHE83, ARG96, ALA256, LEU321, and HEM460 can be regarded as particularly important structural elements contributing to ligand recognition and stabilization within the CYP51 active site (https://www.ebi.ac.uk/pdbe/entry/pdb/1ea1?activeTab=ligands&id=TPF, accessed on 16 September 2026).

The crystal structure of *Candida albicans* CYP51 in complex with itraconazole (1YN) (PDB ID: 5V5Z) was analyzed to characterize the interaction profile of the co-crystallised ligand within the CYP51 active site. Previous structural and computational studies have identified several residues in the CYP51 active site as important for ligand binding, including TYR64, TYR118, PHE126, ILE131, TYR132, PRO230, PHE233, HIS377, MET508, and the heme group (HEM601). When aromatic, hydrophobic, carbon–π, weak hydrogen-bond, and heme-coordination interactions are considered, TYR64, TYR118, PHE126, ILE131, TYR132, PRO230, PHE233, HIS377, MET508, and HEM601 can be considered particularly important structural components contributing to ligand recognition and stabilization within the CYP51 active site. Among these interactions, the aromatic and carbon–π interactions involving TYR118, together with the coordination of the ligand with the heme group, are particularly relevant to the binding mode of itraconazole (https://www.ebi.ac.uk/pdbe/entry/pdb/5v5z?activeTab=ligands&id=1YN, accessed on 16 September 2026).

The crystal structure of *Candida albicans* CYP51 in complex with posaconazole (X2N) (PDB ID: 5FSA) was analyzed to characterize the interaction profile of the co-crystallised ligand within the CYP51 active site. The interaction analysis identified several residues as important for ligand binding, including TYR64, TYR118, PHE126, ILE131, PRO230, PHE233, LEU376, HIS377, PHE380, MET508, and the heme group

(HEM580). When aromatic, hydrophobic, carbon–π, weak hydrogen-bond, sulfur–π, and heme-coordination interactions are considered, TYR64, TYR118, PHE126, ILE131, PRO230, PHE233, LEU376, HIS377, PHE380, MET508, and HEM580 can be considered particularly important structural components contributing to ligand recognition and stabilization within the CYP51 active site (https://www.ebi.ac.uk/pdbe/entry/pdb/5fsa?activeTab=ligands&id=X2N, accessed on 16 September 2026).

2.3 Molecular Docking Protocol

Molecular docking simulations were performed using AutoDock 4.2.6 (17). The docking grid was centered on the binding site of the respective co-crystallised ligand in each CYP51 crystal structure. A grid box of 40 × 40 × 40 points with a spacing of 0.375 Å was used for the docking calculations. For each ligand, including both *R*- and *S*-BTE1 enantiomers and the corresponding co-crystallised reference ligands, a minimum of 50 independent docking runs was performed using the Lamarckian Genetic Algorithm. The docking protocol was validated by re-docking the co-crystallised ligands into their corresponding binding sites. The calculated RMSD values were 0.99 Å for fluconazole (TPF470) in 1EA1, 1.56 Å for itraconazole (1YN) in 5V5Z, and 1.44 Å for posaconazole (X2N) in 5FSA supporting the reliability of the docking protocol. The co-crystallised ligands were retained from their respective crystal structures and subjected to the same docking protocol used for BTE1. Binding interactions and three-dimensional binding poses were visualized using Maestro (Schrödinger, LLC, 2025).

It should be noted that the AutoDock 4.2 scoring function does not explicitly parameterize metal coordination. Interactions are expressed across the heme molecule. Therefore, interactions between the triazole nitrogen and the heme iron were interpreted primarily as geometric observations consistent with the established binding mode of azole antifungal agents rather than as explicitly parameterized energetic contributions to the docking score.

2.4. ADME Prediction

SwissADME was used to predict the physicochemical and pharmacokinetic properties of compound [18-21]. The predicted pharmacokinetic and drug-likeness properties of the compounds were assessed using parameters including Lipinski's Rule of Five, gastrointestinal absorption, blood–brain barrier permeability predicted by the BOILED-Egg model, and overall drug-likeness scores. These parameters were subsequently

analyzed comparatively to evaluate the compounds' potential suitability for oral administration and their overall drug-like profiles.

3 RESULT

For 1EA1 re-docking of the co-crystallised ligand fluconazole (TPF470) reproduced the crystallographic binding modes with RMSD values of 0.99 Å, below the generally accepted threshold of 2.0 Å, indicating that the protocol reproduces the experimental poses reliably. In the *Mycobacterium tuberculosis* CYP51 model, BTE1 was predicted to bind more favourably than fluconazole (TPF470), with docking scores of -10.14, -10.24 and -7.07 kcal/mol respectively for *R*-BTE1, *S*-BTE1 as two enantiomers of BTE1 and Fluconazole (TPF470); the corresponding predicted inhibition constants were 36.74 nM, 31.02 nM and 6.58 μM (Table 1).

For 5V5Z re-docking of the co-crystallised ligand itraconazole (1YN) reproduced the crystallographic binding modes with RMSD values of 1.56 Å, indicating that the protocol reproduces the experimental poses reliably. In the *Candida albicans* CYP51 model, BTE1 was predicted to bind more favourably than itraconazole (1YN), with docking scores of -10.10, -10.33 and -13.35 kcal/mol respectively for *R*-BTE1, *S*-BTE1 as two enantiomers of BTE1 and itraconazole (1YN); the corresponding predicted inhibition constants were 39.46 nM, 27.01 nM and 164.33 pM (Table 2).

For 5FSA re-docking of the co-crystallised ligand posaconazole (X2N) reproduced the crystallographic binding modes with RMSD values of 1.44 Å, indicating that the protocol reproduces the experimental poses reliably. In the *Candida albicans* CYP51 model, BTE1 was predicted to bind more favourably than posaconazole (X2N), with docking scores of -9.82, -9.98 and -14.82 kcal/mol respectively for *R*-BTE1, *S*-BTE1 as two enantiomers of BTE1 and posaconazole (X2N); the corresponding predicted inhibition constants were 63.04 nM, 48.54 nM and 13.62 pM (Table 3).

4 DISCUSSION

Interaction analysis revealed that both BTE1 enantiomers established a broader network of interactions within the CYP51 active site than fluconazole (TPF470), although distinct interaction patterns were observed between *R*-BTE1 and *S*-BTE1. *R*-BTE1 formed π–π interactions with four aromatic residues, namely TYR76, PHE78, PHE83, and PHE255, together with a π–

Table 1. Molecular docking scores, estimated inhibition constants (Ki), and interacting residues according to bond types for the *R*-BTE1, *S*-BTE1 compounds and Fluconazole (TPF470) with 1EA1.

Compounds	Autodock Results				
	Pi-Pi Interaction	**Pi Cation Interaction**	**HydrogenBond**	**Estimated Inhibition, Constant Ki**	**Dock Score (kcal/mol)**
***R*-BTE1**	TYR76 PHE78 PHE83 PHE255	HEM460	ALA256	36.74 nM	-10.14
***S*-BTE1**	TYR76 PHE78 PHE83	HIS259 HEM460	ALA256	31.02 nM	-10.24
TPF470 (Fluconazole)	PHE83 HEM460	-	-	6.58 µM	-7.07

nM:nanomolar, µM:micromolar

Table 2. Molecular docking scores, estimated inhibition constants (Ki), and interacting residues according to bond types for the *R*-BTE1, *S*-BTE1 compounds and Itraconazole (1YN) with 5V5Z.

Compounds	Autodock Results				
	Pi-Pi Interaction	**Pi Cation Interaction**	**HydrogenBond**	**Estimated Inhibition, Constant Ki**	**Dock Score (kcal/mol)**
***R*-BTE1**	HEM601 TYR118	HEM601	-	39.46 nM	-10.10
***S*-BTE1**	HEM601	HEM601	-	27.01 nM	-10.33
1YN (Itraconazole)	TYR64 TYR118	-	-	164.33 pM	-13.35

pM:picomolar, nM:nanomolar

Table 3. Molecular docking scores, estimated inhibition constants (Ki), and interacting residues according to bond types for the *R*-BTE1, *S*-BTE1 compounds and Posaconazole (X2N) **with** 5FSA.

Compounds	Autodock Results				
	Pi-Pi Interaction	**Pi Cation Interaction**	**Hydrogen Bond**	**Estimated Inhibition, Constant Ki**	**Dock Score (kcal/mol)**
***R*-BTE1**	HEM580 PHE233	-	-	63.04 nM	-9.82
***S*-BTE1**	HEM580	HEM580	-	48.54 nM	-9.98
X2N (Posaconazole)	TYR118 HIS377 HEM580	-	-	13.62 pM	-14.82

pM:picomolar, nM:nanomolar

cation interaction involving HEM460 and a hydrogen bond with ALA256. In contrast, *S*-BTE1 exhibited π–π interactions with TYR76, PHE78, and PHE83, while additional π–cation interactions were observed with HIS259 and HEM460, together with a hydrogen bond involving ALA256. Thus, *R*-BTE1 established a greater number of π–π contacts, whereas S-BTE1 displayed an additional interaction with HIS259. Despite these differences, both enantiomers maintained interactions with the heme group and ALA256, which may contribute to their favourable predicted binding profiles. Consistent with these interaction patterns, *S*-BTE1 showed a slightly more favourable docking score (-10.24 kcal/mol) and lower estimated Ki (31.02 nM) than R-BTE1 (-10.14 kcal/mol and 36.74 nM, respectively). In comparison, fluconazole exhibited fewer identified interactions, involving PHE83 and HEM460, and showed a less favourable docking score of -7.07 kcal/mol with an estimated Ki of 6.58 μM. Overall, the results indicate that both BTE1 enantiomers engage the CYP51 active site through multiple complementary interactions, with *S*-BTE1 displaying a modestly more favourable predicted binding profile than *R*-BTE1 (Figure 2-3).

Interaction analysis of the BTE1 enantiomers within the CYP51 active site of the 5V5Z model revealed that both compounds interacted directly with

the heme group (HEM601), although differences were observed in their interaction patterns. *R*-BTE1 established a π–π interaction with TYR118 in addition to a π–cation interaction involving HEM601. In

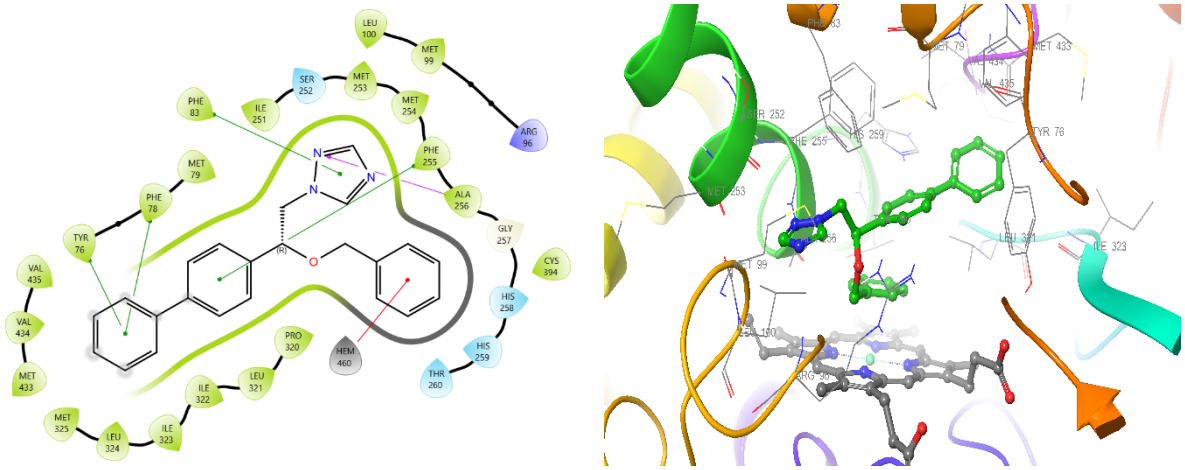

Figure 2. 2D and 3D representation of the interaction areas of the *R*-BTE1 with 1EA1.

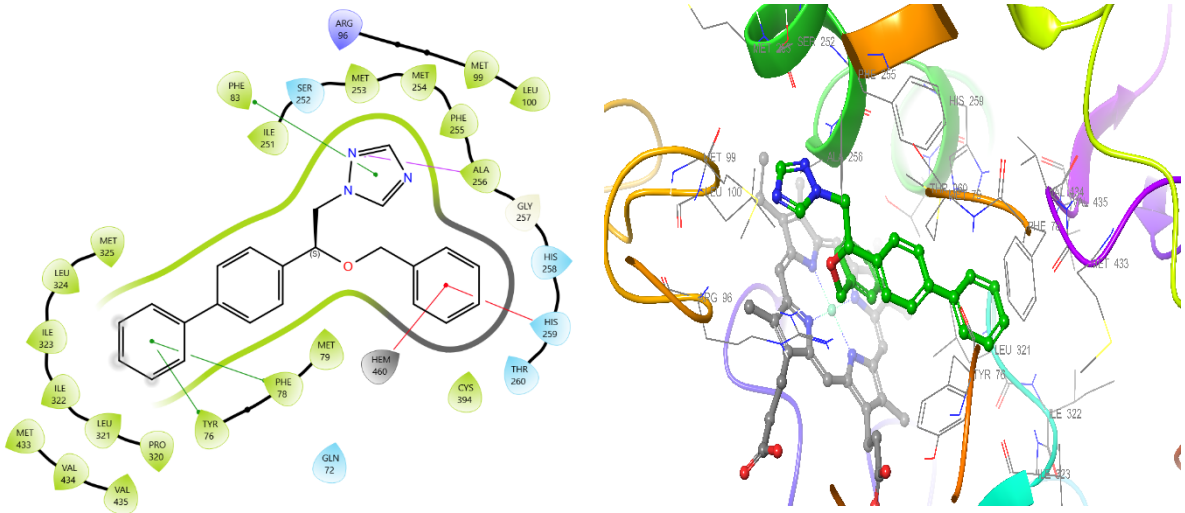

Figure 3. 2D and 3D representation of the interaction areas of the *S*-BTE1 with 1EA1.

contrast, *S*-BTE1 showed a π–cation interaction with HEM601 but no additional π–π interaction with the residues identified for *R*-BTE1. Thus, although *R*-BTE1 exhibited a greater number of identified interactions, *S*-BTE1 showed a slightly more favourable docking score (-10.33 kcal/mol) and a lower estimated Ki value (27.01 nM) compared with *R*-BTE1 (-10.10 kcal/mol and 39.46 nM, respectively). These findings suggest that the differences in the predicted binding affinities of the two enantiomers may not be determined solely by the number of identified

interactions but may also reflect differences in their spatial orientation and interaction geometry within the active site. In comparison,

itraconazole (1YN) formed π–π interactions with TYR64 and TYR118 and exhibited a substantially more favourable docking score (-13.35 kcal/mol) and estimated Ki (164.33 pM) than both BTE1 enantiomers. Overall, both *R*-BTE1 and *S*-BTE1 maintained an interaction with the heme group, while *S*-BTE1 displayed a modestly more favourable predicted binding profile despite the fewer identified interactions (Figure 4-5).

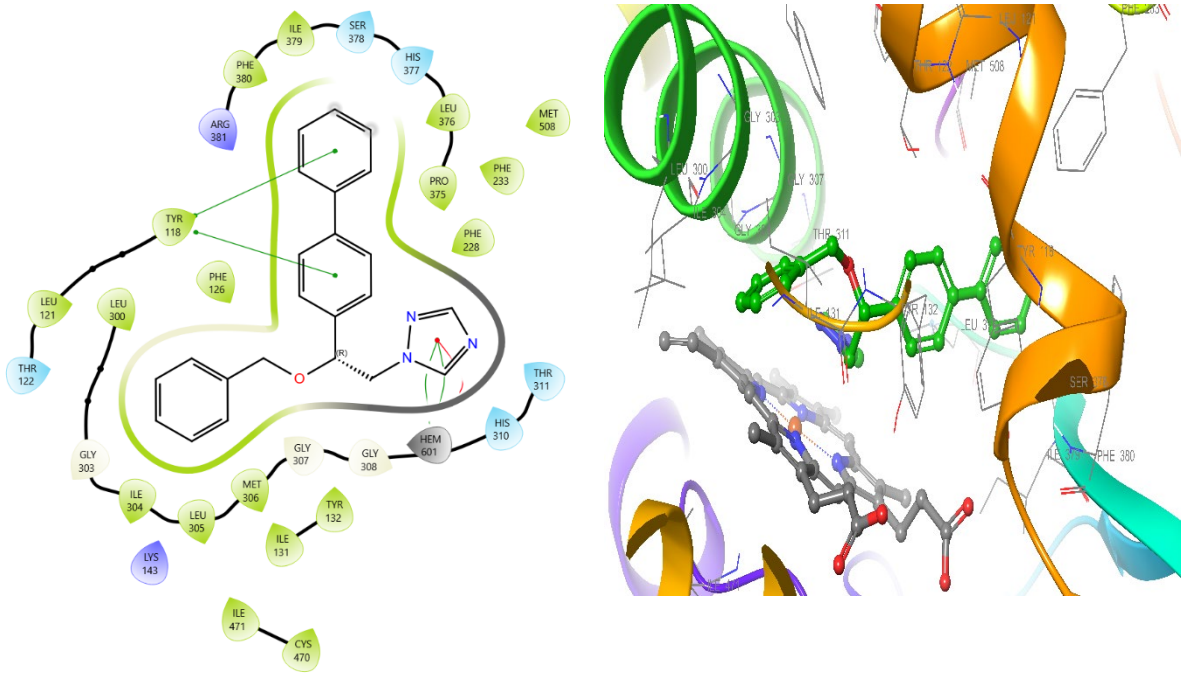

Figure 4. 2D and 3D representation of the interaction areas of the *R*-BTE1 with 5V5Z.

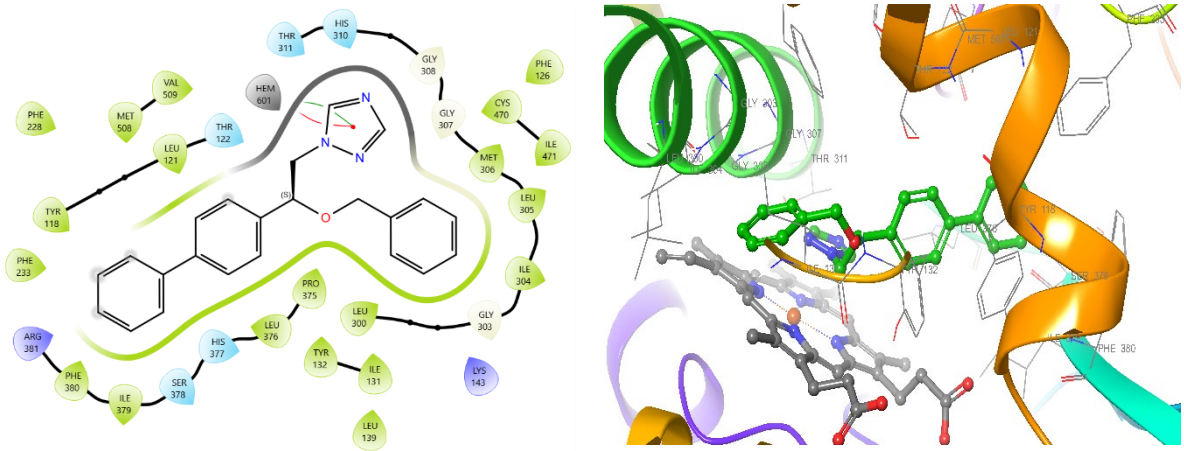

Figure 5. 2D and 3D representation of the interaction areas of the *S*-BTE1 with 5V5Z.

Interaction analysis of the BTE1 enantiomers within the CYP51 active site of the 5FSA model revealed that both compounds established interactions with the heme group (HEM580), although distinct interaction patterns were observed between the two enantiomers. *R*-BTE1 formed a π–π interaction with PHE233 in addition to an interaction involving HEM580, whereas *S*-BTE1 exhibited an interaction with HEM580 without an additional π–π contact with the identified active-site residues. Despite the additional π–π interaction observed for *R*-BTE1, *S*-BTE1 showed a slightly more favourable docking score (-9.98 kcal/mol) and a lower estimated Ki (48.54 nM) compared with R-BTE1 (-9.82 kcal/mol and 63.04 nM, respectively). This finding, consistent with the results obtained for the 5V5Z model, indicates that the predicted binding affinity of the BTE1 enantiomers is not necessarily proportional to the number of identified interactions and may also depend on their spatial orientation and interaction geometry within the binding site. In comparison, posaconazole (X2N) exhibited interactions with TYR118, HIS377, and HEM580 and showed a substantially more favourable docking score (-14.82 kcal/mol) and estimated Ki (13.62 pM) than both BTE1 enantiomers. Overall, both BTE1 enantiomers maintained an interaction with the heme group, while *S*-BTE1 displayed a modestly more favourable predicted binding profile than *R*-BTE1 in the 5FSA model (Figure 6-7).

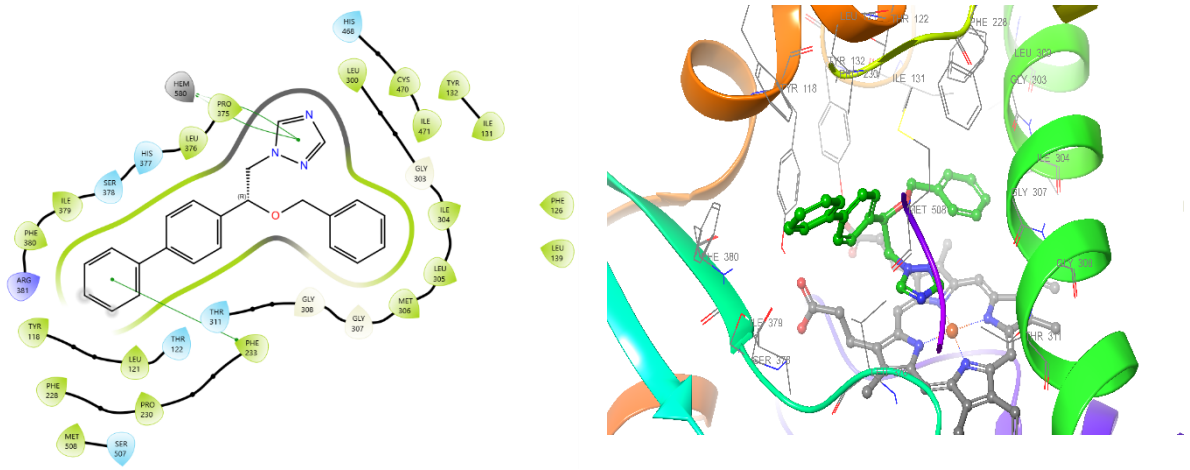

Figure 6. 2D and 3D representation of the interaction areas of the *R*-BTE1 with 5FSA.

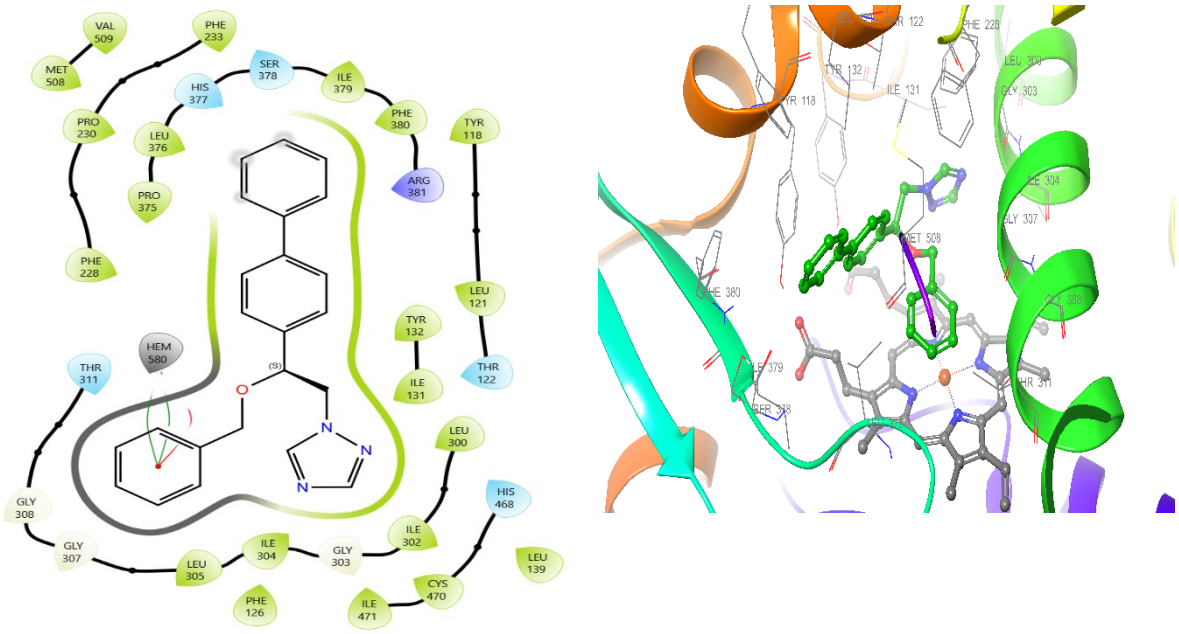

Figure 7. 2D and 3D representation of the interaction areas of the *S*-BTE1 with 5FSA.

Comparison of the docking results for the BTE1 enantiomers across the investigated CYP51 models revealed a consistently more favourable predicted binding profile for S-BTE1 than for R-BTE1. S-BTE1 showed slightly more favourable docking scores and lower predicted Ki values against all three macromolecules, with the most favourable affinity observed for the 5V5Z model (−10.33 kcal/mol; Ki = 27.01 nM). When the BTE1 enantiomers were compared with the corresponding co-crystallised ligands, BTE1 showed more favourable docking scores than fluconazole (TPF470) in the 1EA1 model, whereas itraconazole (1YN) and posaconazole (X2N) exhibited more favourable docking scores than both BTE1 enantiomers in the 5V5Z and 5FSA models, respectively. Although these differences indicate a more favourable predicted binding profile for BTE1 relative to fluconazole, the substantially larger and more structurally complex itraconazole and posaconazole molecules may contribute to their more favourable docking scores through differences in molecular size, flexibility, and the extent of possible protein–ligand interactions. Overall, the comparative docking analysis suggests that *S*-BTE1 has a more favourable predicted binding profile than *R*-BTE1 across the examined CYP51 models, particularly toward the 5V5Z macromolecule (Table 1-3).

Upon examination of the ADME predictions, as shown in Figure 8, the compound was predominantly located within the yellow region of the BOILED-Egg model, indicating a potential for blood-brain barrier permeation, whereas its

position outside the white region suggested limited gastrointestinal absorption. Furthermore, the predicted physicochemical space indicated that the compound largely falls within the region associated with favourable oral bioavailability. Overall, the ADME predictions suggest that the compound exhibits physicochemical properties that may support its oral bioavailability and potential distribution across the blood–brain barrier.

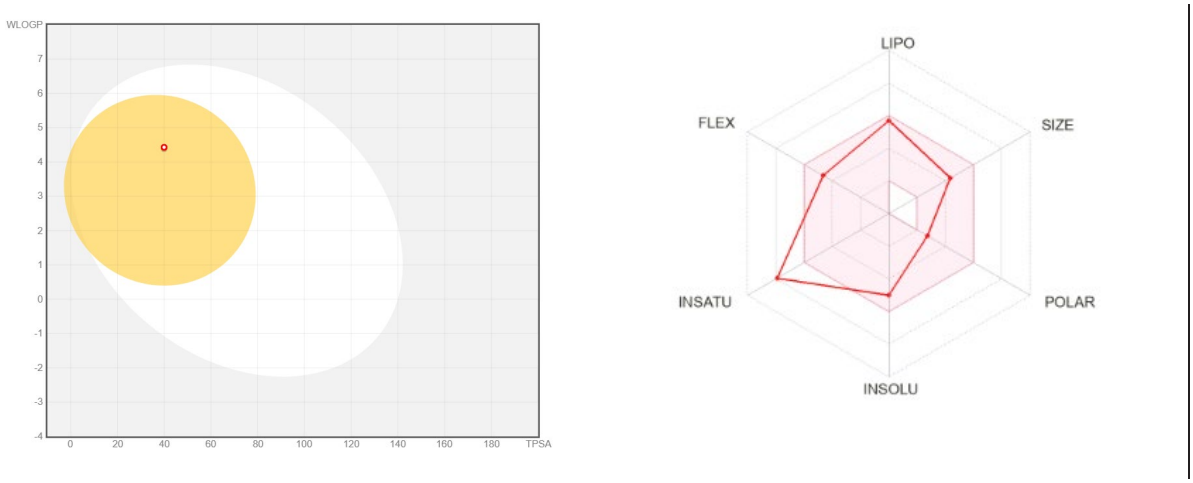

Figure 8. BOILED-Egg model and predicted physicochemical space of BTE1 compound for oral bioavailability.

Several limitations of the present study should be acknowledged. The molecular docking results represent computational predictions, and the AutoDock 4.2 scoring function provides an approximate estimation of binding affinity rather than a direct measure of binding free energy. In addition, the docking protocol treats the receptor as rigid and does not fully account for protein flexibility, explicit solvation, or the coordination characteristics of the triazole nitrogen with the heme iron. Although ADME predictions were also performed to provide preliminary insight into the compound's pharmacokinetic properties, these computational results require experimental validation. Further molecular dynamics simulations and experimental enzymatic and antifungal studies will therefore be important to validate and extend the present findings.

5 CONCLUSION

The novel biphenyl–triazole derivative BTE1 was computationally investigated as a potential CYP51 inhibitor using molecular docking against three CYP51 structures, including Mycobacterium tuberculosis CYP51 (1EA1) and Candida albicans CYP51 models (5V5Z and 5FSA). The applied docking protocol was validated by

redocking the corresponding co-crystallised ligands, which reproduced their experimental binding orientations with RMSD values below the generally accepted threshold of 2.0 Å. Both *R*-BTE1 and *S*-BTE1 were predicted to interact with the CYP51 active site and the heme group, with additional interactions involving key active-site residues. Notably, *S*-BTE1 consistently exhibited slightly more favourable docking scores and lower estimated Ki values than *R*-BTE1 across all three investigated models. The most favourable predicted binding profile among the BTE1 enantiomers was observed for *S*-BTE1 against the 5V5Z model, with a docking score of -10.33 kcal/mol and an estimated Ki of 27.01 nM. Comparison with the co-crystallised azole ligands showed that both BTE1 enantiomers exhibited more favourable docking scores than fluconazole in the 1EA1 model, whereas itraconazole and posaconazole showed more favourable docking scores in the 5V5Z and 5FSA models, respectively. These differences should be interpreted cautiously, as docking scores can be influenced by molecular size, flexibility, and the nature and number of protein-ligand interactions. Nevertheless, the interaction analyses demonstrated that BTE1 can establish multiple complementary contacts within the CYP51 active site, including interactions involving the heme group, supporting the proposed binding mode of the biphenyl-triazole scaffold.

The ADME and drug-likeness analyses further indicated that BTE1 possesses generally favourable physicochemical characteristics and complies with commonly applied drug-likeness criteria, including the Lipinski, Ghose, Veber, Egan, and Muegge rules. The predicted ADME profile also provided preliminary information regarding its potential oral bioavailability and distribution properties. These computational findings collectively support the potential of BTE1 as a CYP51-targeting scaffold and provide a rationale for its further investigation. However, the results remain predictive, and the estimated Ki values should not be considered experimentally determined binding affinities. In addition, the docking approach does not fully account for receptor flexibility, explicit solvation, or the detailed coordination environment of the triazole-heme interaction. Therefore, experimental CYP51 inhibition and antifungal susceptibility studies, together with further computational analyses such as molecular dynamics simulations, will be important to validate the present findings and clarify the biological potential of BTE1 and its enantiomers.

6 FINANCIAL DISCLOSURE

This study was supported by the Research Foundation of ˙Inonu University (grant numbers: TUA-2026-4835), Inonu University, Malatya, Türkiye

7 AUTHOR CONTRIBUTIONS

Hypotesis: Z.Ö; Design: E.S; H.U; B.G; Z.Ö; Literature review: E.S; H.U; B.G; Z.Ö; Data Collection: E.S; H.U; B.G; Z.Ö; Analysis and/or interpretation: E.S; H.U; B.G; Z.Ö; Manuscript writing: E.S; H.U; B.G; Z.Ö.

8 CONFLICTS OF INTEREST

Authors declare that there is no conflict of interest.

9 REFERENCES

[1]. Anandani G, Bhise M, Agarwal A. Invasive fungal infections and the management in immunocompromised conditions. Journal of Family Medicine and Primary Care. Temmuz 2025;14(7):2643-52. doi:10.4103/jfmpc.jfmpc_1582_24

[2]. Lionakis MS, Drummond RA, Hohl TM. Immune responses to human fungal pathogens and therapeutic prospects. Nat Rev Immunol. Temmuz 2023;23(7):433-52. doi:10.1038/s41577-022-00826-w

[3]. Schell WA, Jones AM, Garvey EP, Hoekstra WJ, Schotzinger RJ, Alexander BD. Fungal CYP51 Inhibitors VT-1161 and VT-1129 Exhibit Strong *In Vitro* Activity against Candida glabrata and C. krusei Isolates Clinically Resistant to Azole and Echinocandin Antifungal Compounds. Antimicrob Agents Chemother. Mart 2017;61(3):e01817-16. doi:10.1128/AAC.01817-16

[4]. Lepesheva GI, Friggeri L, Waterman MR. CYP51 as drug targets for fungi and protozoan parasites: past, present and future. Parasitology. Aralık 2018;145(14):1820-36. doi:10.1017/S0031182018000562

[5]. Warrilow AG, Parker JE, Kelly DE, Kelly SL. Azole Affinity of Sterol 14α-Demethylase (CYP51) Enzymes from Candida albicans and Homo sapiens. Antimicrob Agents Chemother. Mart 2013;57(3):1352-60. doi:10.1128/AAC.02067-12

[6]. De Petris A, Crestoni ME, Pirolli A, Rovira C, Iglesias-Fernández J, Chiavarino B, vd. Binding of azole drugs to heme: A combined MS/MS and computational approach. Polyhedron. Nisan 2015;90:245-51. doi:10.1016/j.poly.2015.02.011

[7]. Esfahani A, Omran AN, Salehi Z, Shams-Ghahfarokhi M, Ghane M, Eybpoosh S, vd. Up-regulation of CDR1

and MDR1 efflux pump genes and fluconazole resistance are involved in recurrence in Candida albicans-induced vulvovaginal candidiasis. Diagnostic Microbiology and Infectious Disease. Mayıs 2024;109(1):116242. doi:10.1016/j.diagmicrobio.2024.116242

[8]. Hoy SM. Oteseconazole: First Approval. Drugs. 2022;82(9):1017–1023. doi:10.1007/s40265-022-01734-y.

[9]. Guedes-da-Silva FH, Batista DGJ, Da Silva CF, De Araújo JS, Pavão BP, Simões-Silva MR, vd. Antitrypanosomal Activity of Sterol 14α-Demethylase (CYP51) Inhibitors VNI and VFV in the Swiss Mouse Models of Chagas Disease Induced by the Trypanosoma cruzi Y Strain. Antimicrob Agents Chemother. Nisan 2017;61(4):e02098-16. doi:10.1128/AAC.02098-16

[10]. Han G, Liu N, Li C, Tu J, Li Z, Sheng C. Discovery of Novel Fungal Lanosterol 14α-Demethylase (CYP51)/Histone Deacetylase Dual Inhibitors to Treat Azole-Resistant Candidiasis. J Med Chem. 28 Mayıs 2020;63(10):5341-59. doi:10.1021/acs.jmedchem.0c00102

[11]. Özdemir Z, Zenni YN, Karakurt A, Sari S, Saraç S, Akdağ M, Merde IB, Kart D, Venanzoni R, Flores GA, Angelini P. Potent Antimicrobial Azoles: Synthesis, In Vitro and In Silico Study. Antibiotics. 2024 Nov 4;13(11):1044.

[12]. Karaca E, Özdemir Z, Zenni YN, Karakurt A. Enantioseperation of 2-(1H-imidazol-1-yl)-1-(naphthalen-2-yl) ethan-1-ol which is active metabolite of anticonvulsant nafimidone. Anatolian Journal of Pharmaceutical Sciences. 2023 Dec 12;2(1):85-95.

[13]. Gambacorta N, Özdemir Z, Doğan İS, Ciriaco F, Zenni YN, Karakurt A, Saraç S, Nicolotti O. Integrated experimental and theoretical approaches to investigate the molecular mechanisms of the enantioseparation of chiral anticonvulsant and antifungal compounds. Journal of Molecular Structure. 2022 Dec 15;1270:133905.

[14]. L.M. Podust,T.L. Poulos, & M.R. Waterman, Crystal structure of cytochrome P450 14α-sterol demethylase (CYP51) from Mycobacterium tuberculosis in complex with azole inhibitors, Proc. Natl. Acad. Sci. U.S.A. 98 (6) 3068-3073, https://doi.org/10.1073/pnas.061562898 (2001).

[15]. Keniya MV, Sabherwal M, Wilson RK, Woods MA, Sagatova AA, Tyndall JDA, Monk BC. 2018. Crystal Structures of Full-Length Lanosterol 14α-Demethylases of Prominent Fungal Pathogens Candida albicans and Candida glabrata Provide

Tools for Antifungal Discovery. Antimicrob Agents Chemother 62:10.1128/aac.01134-18. https://doi.org/10.1128/aac.01134-18

[16]. Hargrove, T. Y.; Friggeri, L.; Wawrzak, Z.; Qi, A.; Hoekstra, W. J.; Schotzinger, R. J.; York, J. D.; Guengerich, F. P.; Lepesheva, G. I., Structural analyses of Candida albicans sterol 14α-demethylase complexed with azole drugs address the molecular basis of azole-mediated inhibition of fungal sterol biosynthesis. Journal of Biological Chemistry 2017, 292, (16), 6728-6743.

[17]. Morris, G. M., Huey, R., Lindstrom, W., Sanner, M. F., Belew, R. K., Goodsell, D. S., & Olson, A. J. (2009). AutoDock4 and AutoDockTools4: Automated docking with selective receptor flexibility. Journal of Computational Chemistry, 30(16), 2785–2791.

[18]. A. Daina, O. Michielin, V. Zoete, iLOGP: a simple, robust, and efficient description of n-octanol/water partition coefficient for drug design using the GB/SA approach, J. Chem. Inf. Model. 54 (2014) 3284–3301.

[19]. A. Daina, O. Michielin, V. Zoete, SwissADME: a free web tool to evaluate pharmacokinetics, drug-likeness and medicinal chemistry friendliness of small molecules, Sci. Rep. 7 (2017) 42717.

[20]. A. Daina, V. Zoete, A boiled-egg to predict gastrointestinal absorption and brain penetration of small molecules, ChemMedChem 11 (2016) 1117–1121.

[21]. SwissDrugDesign, (n.d.). http://www.swissadme.ch.